mathematics

MDPI

Article

Multidisciplinary Lightweight Optimization for Front Impact Structure of Body Frame Based on Active and Passive Safety

Tingting Wang *, Mengjian Wang, Xia Li and Dongchen Qin

School of Mechanical and Power Engineering, Zhengzhou University, Zhengzhou 450000, China; mjwang72@163.com (M.W.); jennyhit@163.com (X.L.); dcqin@zzu.edu.cn (D.Q.)
* Correspondence: wangtingting@zzu.edu.cn

Abstract: The Analytic Target Cascading (ATC) is an effective method for solving hierarchical Multidisciplinary Design Optimization (MDO) problems. At the same time, this method suffers from poor convergence and low accuracy, which is caused by the inconsistency of system constraints. In this paper, a novel ATC method based on dynamic relaxation factor is proposed. The dynamic relaxation factor of consistency constraint is added in the system level and is adjusted by the deviation of the linking variables between the levels to ensure the feasible region of the design space. The effectiveness and accuracy of this method are verified by a mathematical example. This method is used to solve the lightweight problem of the trussed front part of the vehicle body frame based on active and passive safety to achieve the collaborative optimization of lightweight trussed frame, crash safety, and aerodynamic characteristics. The important value of the novel ATC method based on dynamic relaxation factor in engineering applications is proven.

Keywords: trussed frame; ATC; dynamic relaxation factor; lightweight; crash safety; aerodynamic characteristics; MDO

Citation: Wang, T.; Wang, M.; Li, X.; Qin, D. Multidisciplinary Lightweight Optimization for Front Impact Structure of Body Frame Based on Active and Passive Safety. *Mathematics* **2021**, *9*, 907. https://doi.org/10.3390/math9080907

Academic Editor: Carlos Llopis-Albert

Received: 22 March 2021
Accepted: 16 April 2021
Published: 19 April 2021

1. Introduction

Formula Student Electric China (FSEC) is a competition which consists of static and dynamic events. Five items are included in the dynamic competition: linear acceleration test, 8-word detour test, high-speed obstacle avoidance test, durability test, and efficiency test. Therefore, it is necessary to comprehensively evaluate the acceleration, durability, and body weight of the racing car. Under the premise of ensuring the personal safety of the driver, the overall performance of the racing car's acceleration, driving range, handling stability, braking, and lightweight is required to be optimal.

The electric racing car in the FSEC is a typical trussed frame structure [1–3]. At present, most scholars only consider the collision safety of the body for lightweight research. In [4], Xiong studied the multi-objective lightweight optimization problem of the front impact structure of the automobile body. The crashworthiness model of the vehicle was established by taking the thickness of the automobile body and the materials as the design variables. In [5], Xie used the thickness of the front cabin of electric automobile as the design variable to design the vehicle lightweight, and verified the safety of the automobile by the simulation of the collision. However, for automobiles, the research of lightweight should not only include passive safety; active safety is also an important factor that cannot be ignored [6,7]. The main problem of active safety is how to improve the handling stability, in addition to being improved by the electronic control safety system [8–11]. In [12], Yu pointed out that the vertical load of the tire on the ground is reduced by the aerodynamic lift on the automobile, and the change of the vertical load has a significant impact on the wheel cornering characteristics, thus affecting the handling stability, as well as the dynamic performance and braking performance of the automobile. Therefore, the research on active safety of racing car can be considered to include aerodynamic characteristics. In [13], the author analyzed the aerodynamic characteristics of Ford F-150 race truck. In order to

change the aerodynamic lift coefficient of the whole vehicle, the modeling design of the truck was adopted, so as to increase the downward pressure of the tire during driving and improve the handling stability of the truck during driving. Aerodynamic characteristics are closely related to the shape of the front of the vehicle [14–16], and are affected by the position of the key nodes in the front of the vehicle. In [17], the author used the key control points of the head shape surface to establish 12 spline curves according to the streamlined head shape of a high-speed train, and then generated seven spline curves for parametric modeling of the head. For the truss body structure, when the node changes, the racing car weight will be affected by the length of the pipe with the change of the node position. Therefore, FSEC racing car is improved in the process of lightweight, which is conducive to improving the active safety and affecting the weight of the racing car.

In general, active and passive safety collaborative optimization is needed to optimize the overall performance of FSEC racing car. The combination of active and passive safety is an effective way to improve vehicle safety. Although many companies and scholars began to pay attention to the research on the combination of active and passive system safety [18,19], the improvement of handling stability in these studies was carried out from the electronic control system. Study of the body structure is ignored, which increases the crash safety and improves the aerodynamic characteristics while lightening, and realizes the integration of active and passive safety. Therefore, this paper studies the abovementioned complex system with multiple couplings from the perspective of structural considerations. The system needs to consider the influence of many disciplines such as the structure, aerodynamic characteristics, and braking performance of the entire vehicle. It is a typical MDO problem, which was formally proposed by the multidisciplinary design optimization technical committee [20]. It fully considers the coordination mechanism between various disciplines in the process of complex product design. It can shorten the design cycle and obtain better design schemes by obtaining the optimal value of conflicting objectives [21–25].

In the study of multidisciplinary optimization engineering problems, MDO optimization method is the key part of MDO research content. It is used to describe the engineering problems involved mathematically. The selection of different types of optimization methods has a great impact on the complexity, accuracy, and calculation time of solution. So far, MDO optimization method has been developed from single-level optimization method to multi-level optimization method. The single-level MDO method is integrated into the system level for design optimization by the design variables and constraints of various sub disciplines, which results in the complexity of the system level. It is not optimized for large-scale engineering cases [26–28]. Therefore, multi-level MDO methods are often used in MDO. It can be decomposed into a number of relatively simple suboptimization problems according to disciplines. The system-level control of global design variables is adopted, and the local design variables are controlled by the subsystem. The difference in optimization results is coordinated by the system level; for example [29–31], Concurrent Subspace Optimization (CSSO), Collaborative Optimization (CO), Bilevel Integrated System Synthesis (BISS), etc. Many new MDO methods have been developed by scholars on the basis of existing MDO optimization methods. In [32], Michelena proposed an ATC method based on component hierarchical decomposition for large-scale system problems according to their structure. This theory provided a reliable method for solving large and complex problems. In [33], Yao considered structural layout, shape, and size optimization, and proposed a Concurrent Subspace Collaborative Optimization method (CSCO). Many design variables do not need to be optimized simultaneously using this method, which significantly reduces the degree of nonlinearity in structural analysis. In [34], Shin and Park proposed the MDO Based on Independent Subspaces (MDOIS) algorithm, which uses a system analysis method to coordinate the coupling relationship between subsystems.

Among them, ATC is used to solve the problem of lightweight and active passive safety comprehensive optimization design of truss body. System decomposition is used to divide a complex system into smaller subsystems and determine the interaction between

them. After decomposition, the different disciplines in the subsystem level are connected with each other by linking design variables, so system coordination must be performed to ensure the convergence of all linking design variables, and the inconsistency of variables between disciplines needs to be considered [35]. In view of the inconsistency between subsystem level, Brauhn [36] used the inequality constraint form to relax the system-level consistency constraints in the CO method, which improved the convergence effect of the CO method. In [37], Li proposed a dynamic relaxation factor method based on the relaxation factor constraint, so that the size of the relaxation factor can be adjusted according to the dynamic inconsistency between disciplines. His theory provides a powerful idea for the research in this paper and is a very useful algorithm. It is used to ensure that the relaxation factor is not only large, but also small, which leads to the failure to meet the relaxation requirements among disciplines and leads to no feasible solution.

In recent years, the intermixing of algorithms has provided a good reference for constructing new algorithms and improving the efficiency of the original ones. In [38], new metaheuristic algorithms are proposed by inserting the model F1 in Slime Mold Algorithm (SMA) and other representative algorithms. In [39], Zapata built a 3D structure using Self-Assembly Algorithm With Particle Swarm Optimization (SAPSO) which is a combination of two emerging techniques (self-assembly and PSO) with the purpose of improving the process of construction of 3D structures and the convergence speed based on decreasing the number of iterations for building any structure. In [40], Roman proposed to mix the Compact Form Dynamic Linearization–Proportional–Derivative Takagi–Sugeno Fuzzy Algorithm (CFDL-PDTSFA) and Virtual Reference Feedback Tuning VRFT to get a new data-driven algorithm of CFDL-PDTSFA-VRFT.

Therefore, in this paper, the idea of dynamic relaxation factor in the CO model is introduced into the ATC model, and the consistency of the linking design variables between the same levels of ATC is used as the dynamic constraint condition. The size of the relaxation factor is adjusted according to the inconsistency of the linking design variables, taking into account the iterative calculation in the optimization process. At the same time, the problem of choosing the size of the relaxation factor is well avoided. However, as the number of iterations increases, the inconsistent information of the linking design variables may be too small and cause the problem to converge incorrectly, so a fixed term is introduced to constrain the lower limit of convergence to ensure the solution feasibility. Then, the dynamic relaxation factor constraint ATC method is used to construct the active and passive safety MDO design platform for the front impact structure of the racing car body, and the polynomial response surface model is used to obtain the analysis models of each level [41] to reduce the calculation time, realize the lightweight of the body frame, and improve the active and passive safety of the whole racing car. It is confirmed that the dynamic relaxation factor ATC method is suitable for practical engineering problems.

2. Materials and Methods

2.1. Multidisciplinary Optimization Model

The CO model is widely used in the MDO method. The main idea of CO is to decompose the complex engineering project system design problem into several subsystem level problems. The design optimization of each subsystem is completed independently without considering the influence of the design results of other subsystems on the system. The incompatibility and inconsistency between subsystems are coordinated by the top system level [31]. It has the characteristics of parallel computing and reduces the difficulty of solving high-order nonlinear equations. However, the algorithm framework is a two-level structure, as shown in Figure 1, which cannot be widely used in all kinds of multi-layer engineering problems, such as automobile manufacturing.

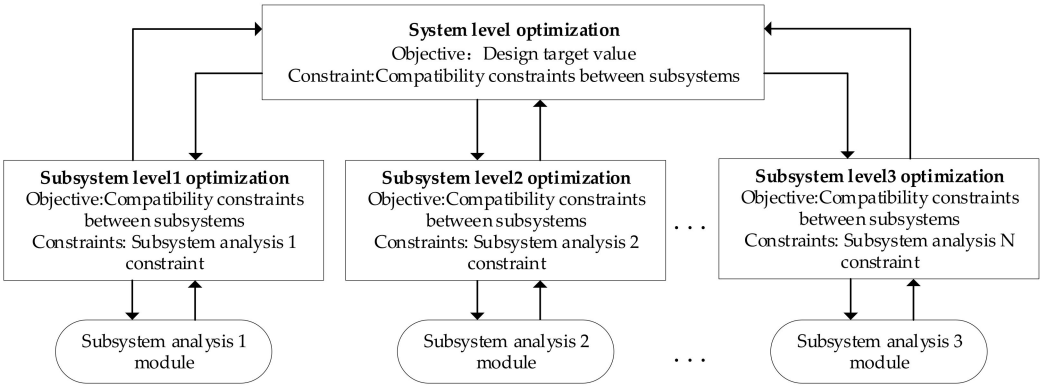

Figure 1. Collaborative optimization method hierarchy.

The ATC method originated from the design of automotive products [32]. The design targets are continuously decomposed from the upper level to the lower level. At the same time, the responses of all levels are continuously fed back from the lower level to upper level. Each unit problem is solved independently; the upper and lower levels overlap for optimization. The optimization process stops when the convergence conditions are satisfied. Therefore, ATC can be applied to infinitely divided i (i = 1, 2, ..., N) level problems. Figure 2 shows the three-level decomposition system.

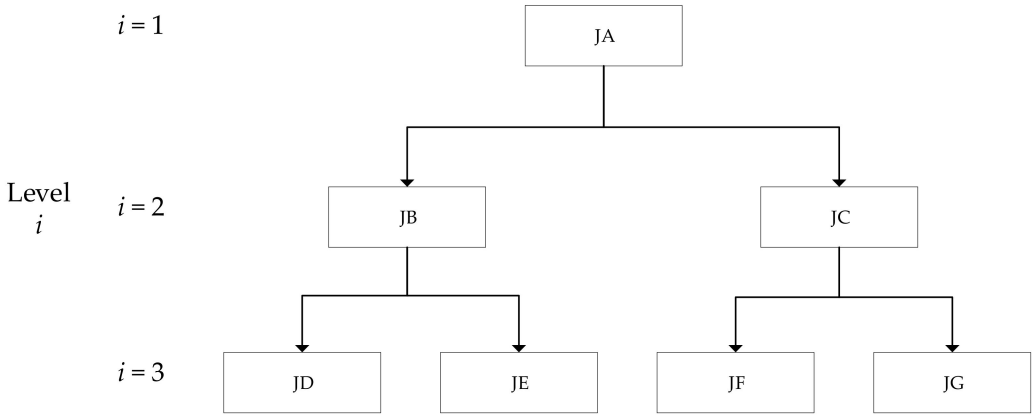

Figure 2. ATC level delivery.

2.2. ATC Model Description

For the automotive industry, a large number of design variables of complete vehicles, systems, subsystems, and parts need to be optimized. The original design problem (vehicle level) can be interpreted as finding a design scheme to minimize the deviation between all design targets and responses on the premise of meeting all constraints, and its mathematical description is shown in Equation (1) [32]:

$$\begin{cases} Min||P-R|| \\ Where \quad R = r(x) \\ s.t. \quad g_i(x,y) \leqq 0 \;\; i = 1,2,\ldots,n \\ \quad\;\; h_i(x,y) = 0 \;\; j = 1,2,\ldots,m \\ \quad\;\; x_{min} \leq x \leq x_{max} \\ \quad\;\; y_{min} \leq y \leq y_{max} \end{cases} \tag{1}$$

The optimized objective function in the Equation (1) is defined as the deviation between the required target P and the system response R obtained by the analysis model.

$r(x)$, $g_i(x,y)$, and $hi(x,y)$ are inequality and equation constraints, x is design variable, y is a linking design variable.

The abovementioned initial design problem is decomposed, and the original problem is divided into multiple hierarchical structures. When using ATC decomposition, the initial targets and constraints in the system level will be decomposed into multiple subsystem spaces. The optimization target P_{ij} at level i is the minimum response deviation calculated by the upper system $(i-1)$ and the lower system $(i+1)$. The optimization target P_{ij} and the analysis model r exist in the target cascading structure. The design variables and parameters, as well as the lower level response, are occupied by the analysis model and return the response of the design problem. Response and linking variables are introduced to describe the interaction between the vertical and horizontal subsystem problems. The response is defined as the output of an analysis model, and the linking variable is defined as a common design that exists between two or more design models. Therefore, the general flowchart of ATC is described [36], as shown in Figure 3.

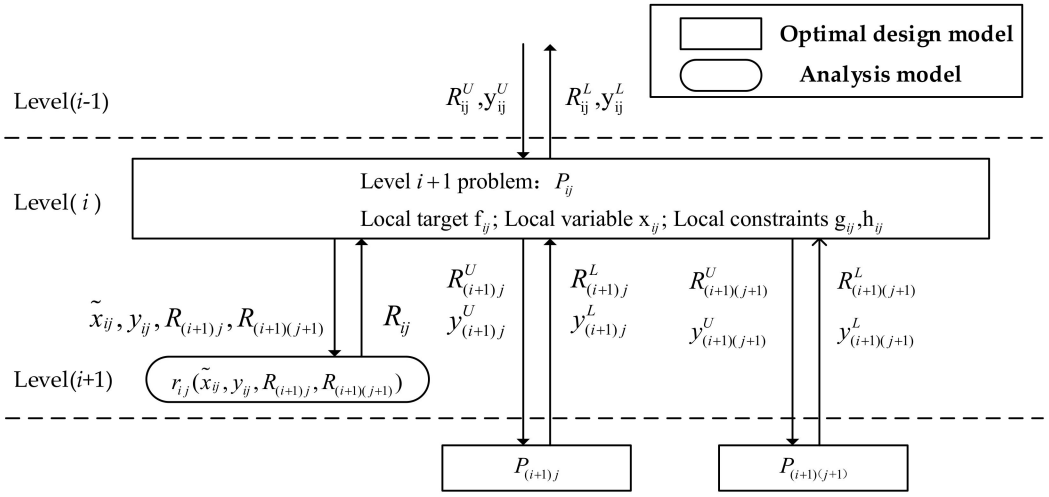

Figure 3. ATC model data flow level transmission design problem.

According to the data transfer flow chart shown in Figure 3, the general ATC model is proposed in this article, as shown in Equation (2).

Level i:

$$\begin{cases} P_{ij}: \ min\omega_{ij}^R \left|\left|R_{ij} - R_{ij}^U\right|\right| + \omega_{ij}^y \left|\left|y_{ij} - y_{ij}^U\right|\right| + \varepsilon_R + \varepsilon_y \\ \quad respect\ to\ \tilde{x}_{ij},\ y_{ij},\ y_{(i+1)j},\ R_{(i+1)j},\ \varepsilon_R,\ \varepsilon_y \\ \quad where,\ R_{ij} = r_{ij}\left(R_{(i+1)j}, \tilde{x}_{ij}, y_{ij}\right) \\ s.t. \quad \omega_{ij}^R \sum_{i=1}^{n} \sum_{j=1}^{c_{(i+1)k}} ||R_{(i+1)j} - R_{(i+1)j}^L||_2^2 \le \varepsilon_R \\ \quad \omega_{ij}^y \sum_{i=1}^{n} \sum_{j=1}^{c_{(i+1)k}} ||y_{(i+1)j} - y_{(i+1)j}^L||_2^2 \le \varepsilon_y \\ \quad g_{ij}\left(R_{ij}, x_{ij}, y_{ij}\right) \le 0 \\ \quad h_{ij}\left(R_{ij}, x_{ij}, y_{ij}\right) = 0 \\ \quad \tilde{x}_{ij}^{min} \le \tilde{x}_{ij} \le \tilde{x}_{ij}^{max}, y_{ij}^{min} \le y_{ij} \le y_{ij}^{max} \end{cases} \tag{2}$$

where P_{ij} is the j-th subsystem optimization problem obtained by the upper level of i $(i = 1, 2, \ldots, n)$, $P_{ij} = \left\{k_1, k_2, \ldots, k_{P_{ij}}\right\}$. R is defined as the response value of the analysis system at this level. R^U, R^L are the target values passed by the upper and lower systems, respectively. y is defined as the linking variable between the same level. y^U, y^L are the linking variables transmitted by the upper and lower systems, respectively. ω represents the weight coefficient value of the response or the linking variable and the matching target importance. ε_R is obtained by the deviation between the target value and the response

value. The number of subproblems in the $(i + 1)$th level is defined as $c_{(i+1)k}$ (k = 1, 2, ..., m). ε_y is obtained by the deviation between the linking variable and the calculated value. r represents the analysis model of the level. $\widetilde{x}_{ij}^{min}$, $\widetilde{x}_{ij}^{max}$ are used as the lower limit and upper limit of the local design variable $\widetilde{x}_{ij}$.

2.3. The Introduction of Dynamic Relaxation Factor in ATC

In the standard ATC optimization method, the deviation between the target and the response is not as small as possible. When the deviation is too small, the Kuhn–Tucker condition may not be met during the calculation process, causing convergence problems. Furthermore, too large will lead to the constraints between the systems being out of control. In [37], Li proposed a dynamic relaxation factor method for the CO algorithm multidisciplinary model based on the fixed relaxation factor, so that the size of the relaxation factor can be self-adjusted according to the inconsistency between disciplines, avoiding excessively large or small case. This mathematical method has brought significant contributions to multidisciplinary optimization, as shown in Equation (3).

$$\varepsilon = (\lambda \times \Delta)^2 \Delta = ||x_{ch1} - x_{ch2}||_2 \, , \; 0.5 < \lambda < 1 \tag{3}$$

where Δ represents the inconsistency between sublevel 1 and sublevel 2. x_{ch1}, x_{ch2} are the design variables optimization solutions from the two subsystems in the optimization process. λ is a constant coefficient, which is used for the system-level optimization problem that determines a feasible region.

In this method, the relaxation factor is adaptively adjusted according to the inconsistent information of the linking variables in each iteration. However, its applicability is limited and only applies when the linking variables are completely consistent.

To improve the consistency of the ATC method, by referring to the method of Equation (3), the tolerance of dynamic linking variables between $i + 1$ system level is constructed as the dynamic relaxation factor constraint of ATC method. In this method, the inconsistency of linking variables among subsystems is taken as the constraint condition. The inconsistency between systems is represented by the deviation of the linking variable γ between levels after each iteration, as shown in Equation (4).

$$\gamma = \sum_{j,k=1}^{n} ||y_{(i+1)j} - y_{(i+1)k}||_2^2 \tag{4}$$

In order to ensure that the optimization problem has a reasonable calculation domain, the coefficient ρ is added to γ, $0.5 \leq \rho \leq 1$. In the early stage of the optimization process, when the inconsistency between the linking variables is large, γ plays a major role in improving the efficiency of the global search in the system-level optimization process. However, in the later stage, when the amount of inconsistency between disciplines γ gradually decreases, then a fixed relaxation term φ is added to the relaxation factor to limit the lower limit of the relaxation factor. It is used to ensure that the system-level optimization problem always has a certain size of feasible region during the dynamic change of the relaxation factor, as shown in Equation (5).

$$\varepsilon_y^* = \rho^2 \gamma + \varphi \tag{5}$$

where $\varphi \in [0.01, \; 0.00001]$, the value of φ depends on the order of magnitude of the variable. For example, when the magnitude of the linking variable is about 10^{-1} and 10^0, we can choose 0.001 as its value, as used in the mathematical example of Equation (9) in this paper. Of course, it is also feasible to choose a smaller value. However, if the value is too small, non-convergence may occur, and appropriate expansion is needed at this time.

The dynamic relaxation factor ATC model is constructed by introducing ε_y^* in the original ATC model. In Equation (6), the dynamic relaxation factor ATC model consisting of system level and subsystem level is shown.

$$\begin{cases} \begin{array}{c} System\ level: \quad min\omega_{ij}^R \left|\left|R_{ij} - R_{ij}^U\right|\right| + \omega_{ij}^y \left|\left|y_{ij} - y_{ij}^U\right|\right| + \varepsilon_R + \varepsilon_y^* \\ respect\ to\ \widetilde{x}_{ij},\ y_{ij},\ y_{(i+1)j},\ R_{(i+1)j},\ \varepsilon_R,\ \varepsilon_y^* \\ where \quad R_{ij} = r_{ij}\left(R_{(i+1)j}, \widetilde{x}_{ij}, y_{ij}\right) \\ \varepsilon_y^* = \rho^2 \sum_{j,k=1}^{n} ||y_{ij} - y_{ik}||_2^2 + \varphi \\ s.t. \quad \omega_{ij}^R \sum_{i=1}^{n} \sum_{j=1}^{c_{(i+1)k}} ||R_{ij} - R_{ij}^L||_2^2 \le \varepsilon_R \\ \omega_{ij}^y \sum_{i=1}^{n} \sum_{j=1}^{c_{(i+1)k}} ||y_{ij} - y_{ij}^L||_2^2 \le \varepsilon_y^* \\ g_{ij}\left(R_{ij}, x_{ij}, y_{ij}\right) \le 0 \\ h_{ij}\left(R_{ij}, x_{ij}, y_{ij}\right) = 0 \\ \widetilde{x}_{ij}^{min} \le \widetilde{x}_{ij} \le \widetilde{x}_{ij}^{max},\ y_{ij}^{min} \le y_{ij} \le y_{ij}^{max} \end{array} \\ \begin{array}{c} Subsystem\ level \quad : min\omega_{ij}^R \left|\left|R_{(i+1)j} - R_{(i+1)j}^U\right|\right| + \omega_{ij}^y \left|\left|y_{(i+1)j} - y_{(i+1)j}^U\right|\right| + \varepsilon_R + \varepsilon_y^* \\ respect\ to\ \widetilde{x}_{(i+1)j},\ y_{(i+1)j} \\ where \quad R_{(i+1)j} = r_{(i+1)j}\left(\widetilde{x}_{(i+1)j}, y_{(i+1)j}\right) \\ s.t. \quad g_{ij}\left(R_{(i+1)j}, x_{(i+1)j}, y_{(i+1)j}\right) \le 0 \\ h_{ij}\left(R_{(i+1)j}, x_{(i+1)j}, y_{(i+1)j}\right) = 0 \\ \widetilde{x}_{(i+1)j}^{min} \le \widetilde{x}_{(i+1)j} \le \widetilde{x}_{(i+1)j}^{max},\ y_{(i+1)j}^{min} \le y_{(i+1)j} \le y_{(i+1)j}^{max} \end{array} \end{cases} \tag{6}$$

where the parameters φ and ρ are selected according to the actual situation in order to ensure the convergence of the algorithm. ε_R is controlled by the system. In this paper, the default weight coefficient ω is 1, which can be adjusted according to the actual weight for different problems.

The calculation process of the dynamic relaxation factor method is shown in Figure 4:

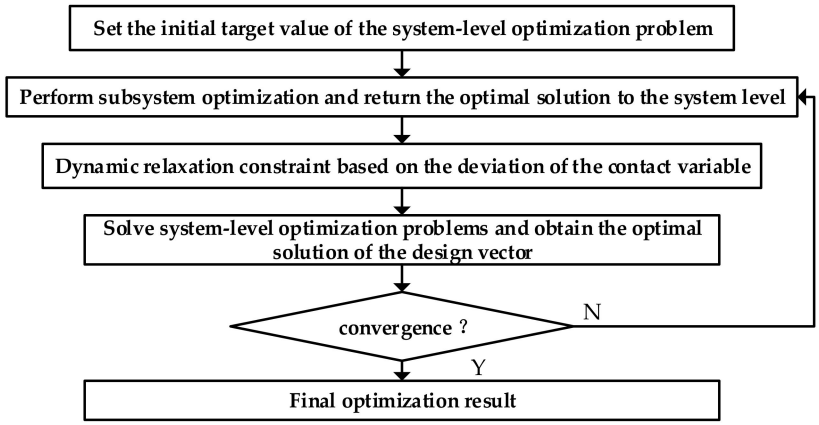

Figure 4. ATC dynamic relaxation factor calculation process.

2.4. Math Problem Application

In order to better prove the ATC method of inter-system linking variable as relaxation factor constraint, a simple mathematical example, Equation (7) [36], is introduced to compare the dynamic relaxation factor and fixed relaxation factor of 0.1, 0.001, and 0.00001,

respectively. This example can be decomposed to make it exist only as related variables, which reduces the difficulty of calculation and can be solved by ATC algorithm.

$$\begin{cases} Min \quad F = x_1^2 + x_2^2 \\ s.t. \ g_1 = x_1 + 0.1x_2 - 4 \leqq 0 \\ \quad g_2 = 2 - 0.1x_1 - x_2 \leqq 0 \\ \quad 0 < x_1 < 5, \ 0 < x_2 < 5 \end{cases} \tag{7}$$

The theoretically optimal solution of this problem is $x^* = (0.19802, 1.9802)$, $f(x^*) = 3.9604$. Aiming at this problem, the traditional fixed relaxation factor ATC optimization method is used as Equation (8):

$$\begin{cases} System\ level: \quad Min \quad F = x_{01}^2 + x_{02}^2 + \varepsilon_1 + \varepsilon_2 \\ Where \quad R_1 = r_1 = 0.5 \times (x_{01}^2 + x_{02}^2), \ R_2 = r_2 = 0.5 \times (x_{01}^2 + x_{02}^2) \\ \quad s.t. \quad (x_{01} - x_{11})^2 + (x_{02} - x_{12})^2 \leqq \varepsilon_1 \\ \quad (x_{01} - x_{21})^2 + (x_{02} - x_{22})^2 \leqq \varepsilon_2 \\ Subsystem\ level\ 1 \quad Min \quad j_1 = (x_{11} - x_{01}^u)^2 + (x_{12} - x_{02}^u)^2 \\ \quad s.t. \quad g_1 = x_{11} + 0.1x_{12} - 4 \leqq 0 \\ Subsystem\ level\ 2 \quad Min \quad j_2 = (x_{21} - x_{01}^u)^2 + (x_{21} - x_{02}^u)^2 \\ \quad s.t. \quad g_2 = 2 - 0.1x_{21} - x_{22} \leqq 0 \end{cases} \tag{8}$$

The inter-discipline consistency constraint is used as the response deviation to construct the dynamic relaxation factor, as shown in Equation (9).

$$\begin{cases} System\ level: \quad Min \quad F = x_{01}^2 + x_{02}^2 + \varepsilon^* \\ Where \quad R_1 = r_1 = 0.5 \times (x_{01}^2 + x_{02}^2), \ R_2 = r_2 = 0.5 \times (x_{01}^2 + x_{02}^2) \\ \quad s.t. \quad (x_{01} - x_{11})^2 + (x_{02} - x_{12})^2 \leqq \varepsilon^* \\ \quad (x_{01} - x_{21})^2 + (x_{02} - x_{22})^2 \leqq \varepsilon^* \\ \quad \varepsilon^* = \rho^2\gamma + \varphi = \rho^2[(x_{11} - x_{21})^2 + (x_{12} - x_{22})^2] + \varphi \\ Subsystem\ level\ 1 \quad Min \quad j_1 = (x_{11} - x_{01}^u)^2 + (x_{12} - x_{02}^u)^2 \\ \quad s.t. \quad g_1 = x_{11} + 0.1x_{12} - 4 \leqq 0 \\ Subsystem\ level\ 2 \quad Min \quad j_2 = (x_{21} - x_{01}^u)^2 + (x_{21} - x_{02}^u)^2 \\ \quad s.t. \quad g_2 = 2 - 0.1x_{21} - x_{22} \leqq 0 \end{cases} \tag{9}$$

The multidisciplinary optimization platform is built into the Isight software; the above problems are solved respectively. The Modified Method of Feasible Directions (MMFD) algorithm is used in the system level, and the Non-Linear Programming by Quadratic Lagrangian (NLPQL) algorithm is used in the subsystem level. The initial values of the above questions are all set to (1,1). The value of ρ as long as it meets the requirements of the value range and the value of φ have been introduced above.

As shown in Figure 5a–c: (a) is the iterative graph of dynamic relaxation factor constraints, (b,c) are the iterative graphs when the relaxation factor is constrained to 0.1 and 0.001. When the relaxation factor is 0.001, there is no feasible solution due to overconstraint.

Table 1 shows the comparison between traditional ATC and ATC based on dynamic relaxation factor. As shown in Table 1, when the relaxation factor is 0.1 for optimization, the constraint strength is insufficient, which leads to premature convergence, with a large error of 28.79%; when the relaxation factor is 0.001, the optimal value is close to the theoretical solution and the difference is only 2.04%, but there is still a 0.83% gap compared with the dynamic relaxation factor; when the relaxation factor is 0.00001, the relaxation factor constraint is too small, resulting in no feasible solution. In addition, when the dynamic relaxation factor is used for iteration, the number of iterations is only 17 times. Compared with the relaxation factor of 0.1, the number of iteration steps is reduced by three steps, and compared with the relaxation factor of 0.001, it is reduced by 17 steps.

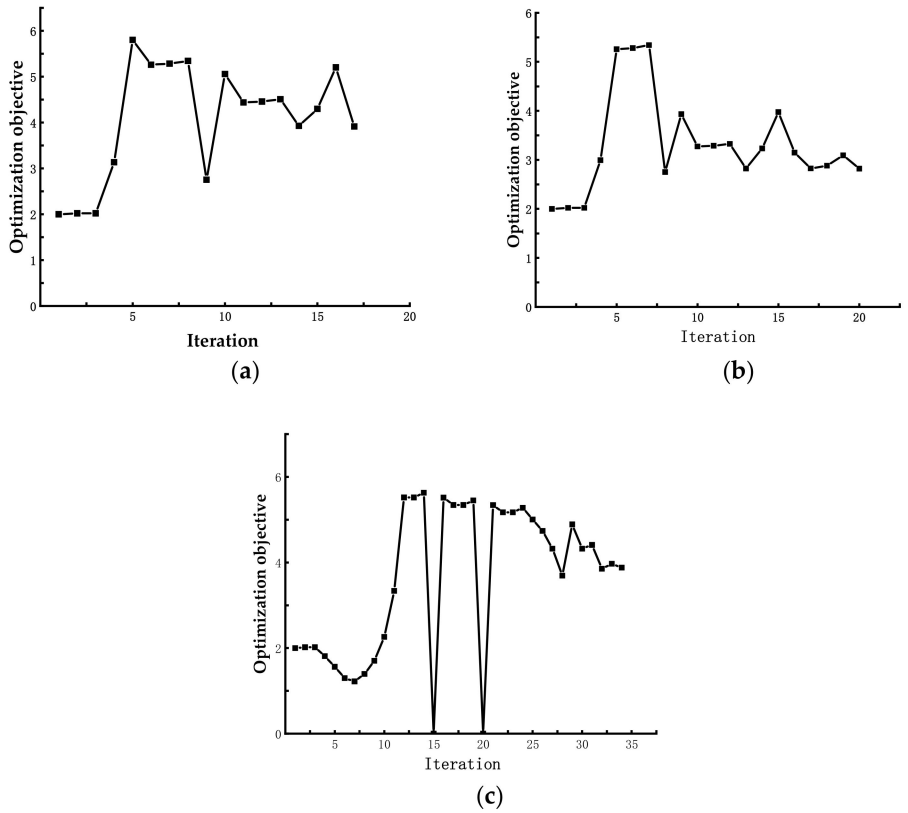

Figure 5. Different relaxation factor iteration; (**a**) dynamic relaxation factor constraints; (**b**) the relaxation factor is constrained to be 0.1; (**c**) the relaxation factor is constrained to be 0.001.

Table 1. Comparison between traditional ATC and dynamic relaxation factor ATC.

Solve under Different Conditions	Optimal Solution	Error Accuracy	Number of Iterations
Theoretical solution	3.9604	——	——
Solution with a relaxation factor of 0.1	2.8204	28.79%	20
Solution with a relaxation factor of 0.001	3.8796	2.04%	34
Solution with a relaxation factor of 0.00001	No feasible solution	——	——
Dynamic relaxation factor	3.9125	1.21%	17

Therefore, dynamic relaxation factor constraints are adopted to avoid constraints and insufficient constraints when selecting relaxation factor constraints, and to improve the efficiency and accuracy of the solution.

3. Engineering Problem Solving

Lightweight optimization for front impact structure of body frame based on active and passive safety is a typical ATC problem. Before the problem is stratified, the optimization objective is lightweight, and the constraints are collision safety and air lift. The research object of this problem is the original truss body, as shown in Figure 6. It is a typical MDO problem to study the lightweight of a truss body while ensuring active and passive safety, which involves many design variables and constraints. Since the linking variables of the two disciplines, crash safety and air lift, are the length and wall thickness of critical pipe fittings, which have a direct impact on lightweighting, the above unstratified problem can be decoupled into a two-level ATC problem.

Figure 6. Electric formula racing.

Therefore, the ATC method is used to decompose the complex engineering system into several subsystems for optimization, which can eliminate the complex system analysis and optimize each subsystem in parallel, reducing the complexity of the whole system. However, auxiliary variables are added in the process of optimization, which also increases the calculation of the whole system to a certain extent, so it is very important to apply efficient optimization algorithm to each subsystem of ATC for optimization calculation. At the same time, the response surface model is used to overcome the problems of spending a lot of time and energy on simulation calculations and low efficiency in finite element simulation analysis.

3.1. Passive Safety

The truss body established in this paper is based on a certain electric formula, combined with the design requirements in the competition rules and created by SolidWorks software. Considering the truss body's passive safety, materials, processing technology, cost, and other aspects, the pipe fittings of truss body are divided into seven specifications, as shown in Figure 7.

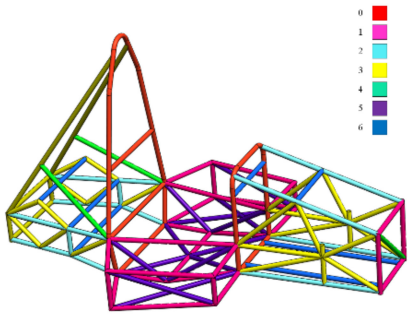

Figure 7. Grouping of pipe fittings.

Since (0) the main ring and the front ring are important structures of the truss body, the size specifications and material requirements are relatively strict. They are not used as design variables to ensure the strength and rigidity of the frame structure. The thickness of the pipe fittings (1)–(6) is shown in Table 2 as the design variable t_i ($i = 1, 2, \ldots, 6$).

During the collision, the deformation of the driver's cockpit should be reduced as far as possible to ensure that the driver has enough living space; the deformation of the front cabin and the motor transmission cabin should be allowed to absorb the kinetic energy transmitted by the body when the collision occurs, so as to reduce the collision acceleration of the cockpit and reduce the impact damage to the driver caused by the collision impact. For passenger cars, a major cause for the injury of the passenger's leg is that there is body front panel intrusion in the frontal rigid collision. Therefore, the deformation of body front panel which is in contact with the front end of the driver should be reduced as much as possible. This will lead to the driver's leg injury being small and easy escape [5,42].

Table 2. Main parameters of racing rods.

Main Components (Design Variables)	Initial Value/mm	Design Upper Limit/mm	Design Lower Limit/mm	Material
(0) Front ring and main ring	1.6	-	-	4130 steel
(1) Front baffle, roll cage diagonal brace, main ring diagonal brace, side anti-collision structure, battery protection structure	1.6	2.0	1.2	4130 steel
(2) The upper and lower supports of the front clapboard and the upper and lower longitudinal pipes of the motor drive cabin	3.5	4.5	3.0	6061 aluminum
(3) Truss support pipe for front cabin and motor drive cabin	3.5	4.5	3.0	6061 aluminum
(4) Front partition support and main ring support	1.5	1.6	1.5	4130 steel
(5) Cockpit and battery protection structure truss support pipe	1.6	2.0	1.2	4130 steel
(6) Mounting cross bar for motor, differential, and drive	1.2	1.6	0.9	4130 steel

Therefore, in the simulation analysis of the frontal crash safety of the racing car, the intrusion at body front panel and the peak acceleration of the cockpit are two important evaluation indicators.

3.2. Active Safety

In the process of vehicle driving, the vertical load of tire is often changed. The cornering characteristic of tire is affected by the change of vertical load, which leads to the change of handling and stability. As shown in Figure 8, there is the influence of different vertical loads on the cornering stiffness of A-70 series tires, B-high performance 70 series tires, and C-60 series tires [12].

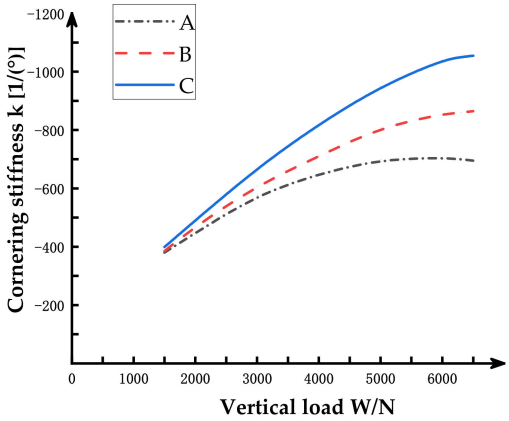

Figure 8. Cornering stiffness of different series of tires.

Therefore, the vertical load of the air lift tire can be changed by the air lift, which affects the handling and stability of the vehicle to a certain extent. At present, many rail vehicles have been designed for the front part of the vehicle [43,44] to increase the air pressure and reduce the air resistance. In order to reduce the amount of calculation, this paper only designs the head of the truss car body. The front model is established and the aerodynamic characteristics of the front part are optimized to increase the negative pressure during the driving of the front part.

The vertical component of the vehicle becomes the aerodynamic lift during driving. The aerodynamic lift is proportional to the square of the incoming flow velocity, the

windward area of the racing car, and the air lift coefficient C_l. The air lift coefficient expression is shown in Equation (10):

$$C_l = \frac{F_z}{2\rho v_\infty^2 S} \tag{10}$$

where S, v, ρ are defined as windward area, incoming flow velocity, and air density.

The head of the truss body is shown in Figure 9. Pipe fitting 1, pipe fitting 2, and pipe fitting 3 are the longitudinal pipe of body front panel, the middle pipe under the front diaphragm, and the transverse pipe of body front panel. Considering the influence of the body structure on active safety, the length change Δl_j ($j = 1, 2, 3$) of three pipe fittings is taken as the design variable and the length of other members is changed according to the position relationship.

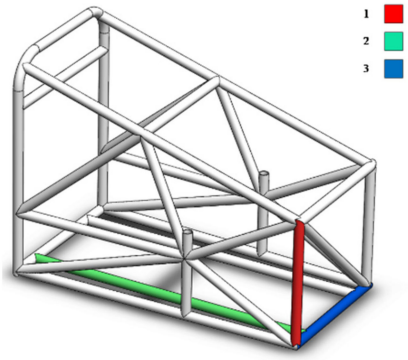

Figure 9. Truss body head pipe fittings.

As shown in Table 3, the negative and positive signs are represented as length decrease and length increase. According to the position of the front pipe fittings, the parametric design of the front shape is shown in Figure 10. According to the Computational Fluid Dynamics (CFD) simulation analysis, the aerodynamic characteristics are greatly affected by the concave and convex of the curve at the top of the vehicle head, and the height change value Δdy at the midpoint of the longitudinal symmetry plane of the vehicle head is taken as the design variable.

Table 3. Selection of design variable parameters for front part.

Design Variable	Initial Value/mm	Lower Limit/mm	Upper Limit/mm
Change value of length of tube 1	0	−5.0	30.0
Change value of length of tube 2	0	−50.0	75.0
Change value of length of tube 3	0	−25.0	15.0
Change value of longitudinal symmetry plane of the vehicle head	0	−20.0	25.0

The change range curve at the midpoint of the longitudinal symmetry plane is shown in Figure 11. For the points between the longitudinal midpoint and the two ends, the coordinate increment value is changed according to the linear law. The deformation is mainly the change of the unevenness of the curve. The two end points of the control line need to be fixed. The change from the endpoints at both ends to the midpoint of the control line is increasing. When Δdy < 0, the curve is concave inward, and when Δdy > 0, the curve is convex outward. The air lift coefficients at different locations are shown in Figure 12.

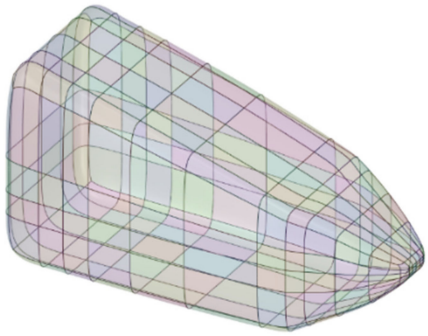

Figure 10. Shape design of the front part.

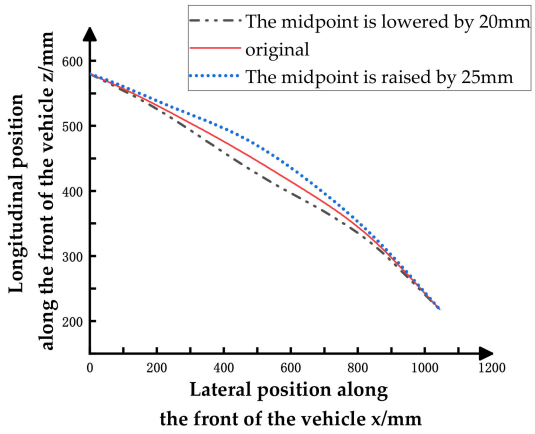

Figure 11. The change range of the midpoint of longitudinal symmetry plane of the vehicle head.

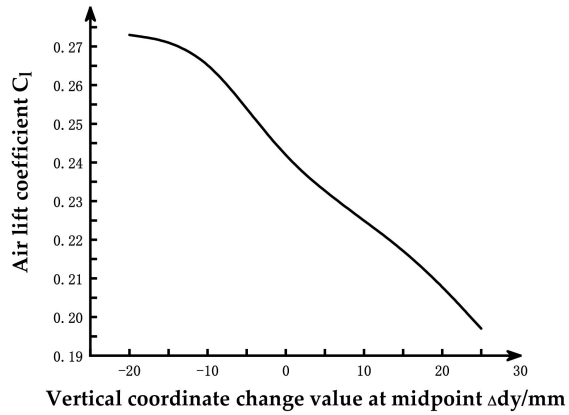

Figure 12. Air lift coefficients at different locations of the midpoint.

To make the incoming flow uniform and stable, the wake flow is fully developed, and the calculation domain is too small to avoid backflow. This paper sets the calculation domain of the cuboid as 4 times the head length of the front part, 8 times the head length of the rear part, 6 times the head height of the upper part, and 6 times the head width of the left and right parts, as shown in Figure 13.

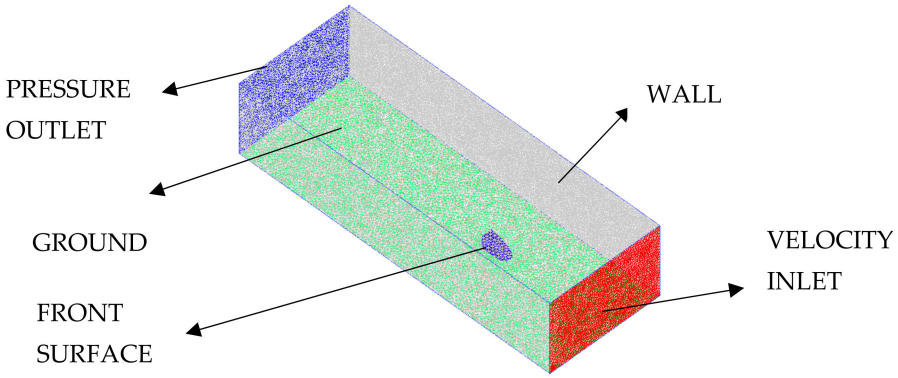

Figure 13. Setting of computational domain for CFD simulation of vehicle head.

ICEM software is used to treat the geometric surface, and tetrahedral mesh elements are selected. Encrypt the grid near the front of the racing car to ensure calculation accuracy [2]. The basic parameter settings are shown in Table 4:

Table 4. Basic parameters of CFD simulation.

Calculation Domain Boundary Type	Parameter Setting
VELOCITY INLET	$v = 11.1$ m/s
PRESSURE OUTLET	Free pressure outlet, hydraulic diameter: 2.04 m, turbulence intensity: 5%
GROUND	Slip wall, $v = 11.1$ m/s
WALL	
FRONT SURFACE	Immovable avoidance surface

3.3. Engineering Problem ATC Model

To sum up, in order to meet the lightweight needs of the automotive industry, as shown in Equation (11):

$$\begin{gathered} \text{Find}: t_i, \Delta l_j, \ \Delta\text{dy} \\ \text{Objective}: \ Min\ \text{M}\left(t_i, \Delta l_j\right) \\ \text{s.t.} \quad G_A\left(t_i, \Delta l_j\right) = \text{A} - 60 \le 0 \\ G_D\left(t_i, \Delta l_j\right) = \text{D} - 71.6 \le 0 \\ G_{Cl}\left(\Delta l_j, \ \Delta\text{dy}\right) = minC_l\left(\Delta l_j, \ \Delta\text{dy}\right) \\ t_i^{min} \le t_i \le t_i^{max} \\ \Delta l_j^{min} \le \Delta l_j \le \Delta l_j^{max} \\ \Delta\text{dy}^{min} \le \Delta\text{dy} \le \Delta\text{dy}^{max} \\ i = 1, 2, \ldots, 6; j = 1, 2, 3 \end{gathered} \tag{11}$$

where A is the peak acceleration during the collision, D is the intrusion at body front panel during the collision, M is the weight of the truss body, C_l is the air lift coefficient, t_i is the pipe thickness, l_i is the pipe length, Δdy is the change value of midpoint height of longitudinal symmetry plane. According to the calculation framework of the ATC method, the active and passive safety car body crashworthiness structure optimization problem is decomposed into a system-level optimization (lightweight system) and three subsystems (intrusion subsystem, peak acceleration subsystem, and air lift coefficient subsystem) optimization problems. At the same time, the dynamic relaxation factor model is introduced into the ATC method framework. The mathematical description is as follows in Equations (12)–(15):

System level:

$$\begin{cases} Min \;\; P = M(t_i, \Delta l_j) + \varepsilon_{RCl} + \varepsilon_A + \varepsilon_D + \varepsilon_{Cl} \\ \omega_{RCl}||C_{Cl} - C_{Cl}^L||_2^2) \;\leq \varepsilon_{RCl} \\ \omega_A||y_A - y_A^U||_2^2 \leq \varepsilon_A \\ \omega_D(||y_D - y_D^U||_2^2 \leq \varepsilon_D \\ \omega_{Cl}||y_{Cl} - y_{Cl}^U||_2^2 \leq \varepsilon_{Cl} \\ \varepsilon_A = \left(\rho_A^2 \times \left|\left|t_A - t_D\right|\right|_2^2 + \left|\left|\Delta l_A - \Delta l_D\right|\right|_2^2 + \varphi_A\right) \\ \varepsilon_D = \left(\rho_D^2 \times \left|\left|t_A - t_D\right|\right|_2^2 + \left|\left|\Delta l_A - \Delta l_D\right|\right|_2^2 + \varphi_D\right) \\ \varepsilon_{Cl} \;= \left(\rho_{Cl}^2 \times ||\Delta l_A - \Delta l_{Cl}||_2^2 + ||\Delta l_B - \Delta l_{Cl}||_2^2 + \varphi_{Cl}\right) \end{cases} \tag{12}$$

Subsystem level:
Analysis model of peak acceleration at impact:

$$\begin{cases} Min \quad J1 = \omega_A||y_A - y_A^L||_2^2 \\ \text{s.t.} \;\; G_A = A - 60 \leq 0 \\ y_A = \left[\Delta l_j, t_i\right] \\ \Delta l_i^{min} \leq \Delta l_i \leq \Delta l_i^{max} \\ \Delta l_j^{min} \leq \Delta l_j \leq \Delta l_j^{max} \end{cases} \tag{13}$$

Analysis model of intrusion at body front panel:

$$\begin{cases} Min \quad J2 = \omega_D(||y_D - y_D^L||_2^2) \\ \text{s.t.} \;\; G_D = D - 71.6 \leq 0 \\ y_D = [\Delta l_i, t_i] \\ t_i^{min} \leq t_i \leq t_i^{max} \\ \Delta l_j^{min} \leq \Delta l_j \leq \Delta l_j^{max} \end{cases} \tag{14}$$

Analysis model of air lift coefficient:

$$\begin{cases} Min \quad J3 = \omega_{Cl}(\left|\left|y_{Cl} - y_{Cl}^U\right|\right|_2^2 + \omega_{RCl}\left|\left|C_{Cl} - C_{Cl}^L\right|\right|_2^2) \\ \text{s.t.} \;\; G_{Cl} = minC_{Cl} \\ C_{Cl} = R(\Delta \text{dy}, \Delta l_j) \\ y_{cl} = \left[\Delta l_j\right] \\ \Delta l_j^{min} \leq \Delta l_j \leq \Delta l_j^{max} \\ \Delta \text{dy}^{min} \leq \Delta dy \leq \Delta \text{dy}^{max} \end{cases} \tag{15}$$

where y represents the linking variables of different models, and the superscripts U and L represent the system level and the subsystem level. C is the analysis model, which is obtained through the fluid subsystem analysis module. ε_D, ε_A, ε_{Cl} are defined as the inter-system linking deviation of intrusion, peak acceleration, and air lift coefficient.

3.4. Multidisciplinary Optimization

In order to accurately establish a Response Surface Methodology (RSM), a Design of Experiment (DOE) is usually used to sample the design space. Among the many DOE methods, the Optimal Latin Hypercube Design (Opt LHD) improves the uniformity of the random Latin Hypercube Design, making the fitting of factors and responses more accurate and true. The Opt LHD makes all the test points evenly distributed in the design space as much as possible, with excellent space filling and balance.

Generally speaking, the first-order RSM has a simple structure and requires relatively little test data, but the accuracy of the RSM is low. The combined effect is poor and cannot

reflect the interaction between the independent variables. Second-order polynomial RSM is used to make up for this defect as Equation (16) is generally used [41]:

$$\hat{Y} = b_0 + \sum_{i=1}^{n} b_i x_i + \sum_{i=1}^{n} \sum_{j=1}^{n} b_{ij} x_i \tag{16}$$

where b_0, b_i, b_{ij} are the undetermined constant term, the first coefficient term, and the quadratic coefficient of the polynomial. $\hat{Y}$ is the fitting response of the polynomial response surface. Y is the real function response, and x_i $(i = 1, 2 \ldots, n)$ is the design variable.

The Opt LHD is used to extract 16 groups of sample points from 10 design variables, t_i, Δl_j, Δdy. The vehicle weight (M), intrusion (D), peak acceleration (A), and air lift coefficient (C_l) are taken as the target response. M and D are solved by LS-DYNA software, C_l is solved by Fluent software, the results are shown in Table 5.

Table 5. Sampling data and simulation response value.

Design Variable	**1**	**2**	**3**	**4**	**5**	**6**	**7**	**8**
t_1/mm	1.68	1.65	1.81	2.00	1.84	1.92	1.89	1.87
t_2/mm	3.97	4.03	4.30	3.83	3.77	4.17	3.57	3.90
t_3/mm	4.23	3.50	4.30	4.43	4.37	3.77	3.90	3.83
t_4/mm	1.51	1.50	1.60	1.54	1.58	1.53	1.51	1.53
t_5/mm	1.95	1.76	1.92	1.87	1.60	2.00	1.71	1.63
t_6/mm	1.95	1.81	1.79	1.89	1.73	1.71	1.68	2.00
Δl_1/mm	−14.00	−6.67	−21.33	4.33	26.33	−17.67	30.00	−3.00
Δl_2/mm	0.00	−33.33	41.67	16.67	25.00	58.33	−8.33	75.00
Δl_3/mm	15.00	−3.67	−9.00	−25.00	7.00	−19.67	−14.33	9.67
Δdy/mm	−2.00	−17.00	−14.00	−11.00	16.00	13.00	1.00	−5.00
M/kg	46.43	45.77	45.85	47.79	49.22	48.81	47.52	43.84
D/mm	50.19	49.57	50.13	62.90	50.16	62.26	64.71	63.83
A/g	48.42	45.75	49.84	50.93	48.25	50.00	47.76	48.94
C_l	0.26	0.30	0.25	0.25	0.23	0.23	0.24	0.21
Design Variable	**9**	**10**	**11**	**12**	**13**	**14**	**15**	**16**
t_1/mm	1.71	1.95	1.63	1.79	1.73	1.97	1.76	1.60
t_2/mm	4.10	3.70	4.43	4.23	3.50	4.50	4.37	3.63
t_3/mm	3.70	3.63	4.17	4.50	4.10	3.97	3.57	4.03
t_4/mm	1.57	1.59	1.55	1.52	1.56	1.55	1.57	1.59
t_5/mm	1.73	1.84	1.65	1.81	1.97	1.68	1.89	1.79
t_6/mm	1.60	1.84	1.87	1.63	1.65	1.76	1.97	1.92
Δl_1/mm	15.33	8.00	11.67	19.00	−10.33	−25.00	22.67	0.67
Δl_2/mm	66.67	−41.67	8.33	33.33	50.00	−16.67	−25.00	−50.00
Δl_3/mm	11.67	1.67	−17.00	−1.00	4.33	−6.33	12.33	−22.33
Δdy/mm	4.00	19.00	25.00	−20.00	22.00	10.00	−8.00	7.00
M/kg	46.66	39.19	43.04	43.08	45.20	41.43	45.85	51.78
D/mm	65.43	67.00	70.84	66.51	69.77	78.54	71.04	65.10
A/g	46.86	48.49	47.23	49.10	47.85	49.05	48.71	47.59
C_l	0.20	0.29	0.24	0.24	0.23	0.28	0.27	0.32

The RSM of the vehicle mass (M), the intrusion (D), the peak acceleration (A), and the air lift coefficient (C_l) are obtained, following Equations (17)–(20):

$$\begin{gathered} M = 50.779 - 0.102 * \Delta l_1 - 0.041 * \Delta l_2 + 0.032 * \Delta l_3 - 0.0248 * t_1 - 0.002 * t_2 - 0.014 * t_3 - 0.015 * t_4 + 0.003 * t_5 - \\ 0.001 * t_6 + 0.001 * \Delta l_1 * \Delta l_2 + 0.001 * \Delta l_1 * \Delta l_3 + 0.412 * \Delta l_1 * t_1 - 0.234 * \Delta l_1 * t_2 - 0.04 * \Delta l_1 * t_3 + 0.047 * \Delta l_1 * t_4 - \\ 0.286 * \Delta l_1 * t_5 + 0.189 * \Delta l_1 * t_6 + 0.01 * \Delta l_2 * \Delta l_2 + 0.001 * \Delta l_2 * \Delta l_3 + 0.049 * \Delta l_2 * t_1 - 0.106 * \Delta l_2 * t_2 + 0.018 * \Delta l_2 * t_3 + \\ 0.076 * \Delta l_2 * t_4 - 0.071 * \Delta l_2 * t_5 - 0.084 * \Delta l_2 * t_6 + 0.006 * \Delta l_3 * \Delta l_3 + 0.33 * \Delta l_3 * t_1 - 0.303 * \Delta l_3 * t_2 + 0.057 * \Delta l_3 * t_3 - \\ 0.096 * \Delta l_3 * t_4 - 0.046 * \Delta l_3 * t_5 + 0.06 * \Delta l_3 * t_6 - 0.087 * t_1 * t_1 - 0.046 * t_1 * t_2 - 0.122 * t_1 * t_3 - 0.116 * t_1 * t_4 - 0.038 * t_1 * t_5 \\ - 0.038 * t_1 * t_6 - 0.006 * t_2 * t_2 - 0.024 * t_2 * t_3 - 0.033 * t_2 * t_4 + 0.004 * t_2 * t_5 - 0.003 * t_2 * t_6 - 0.123 * t_3 * t_3 - 0.122 * t_3 * t_4 \\ - 0.011 * t_3 * t_5 - 0.022 * t_3 * t_6 - 0.114 * t_4 * t_4 - 0.012 * t_4 * t_5 - 0.022 * t_4 * t_6 + 0.009 * t_5 * t_5 + 0.003 * t_5 * t_6 - 0.001 * t_6 * t_6 \end{gathered} \tag{17}$$

$$D = 24.433 + 0.474 * \Delta l_1 + 0.121 * \Delta l_2 - 0.169 * \Delta l_3 + 0.075 * t_1 + 0.012 * t_2 + 0.061 * t_3 + 0.044 * t_4 - 0.017 * t_5 - 0.001 * t_6 + 0.004 * \Delta l_1 * \Delta l_1 + 0.003 * \Delta l_1 * \Delta l_2 - 0.001 * \Delta l_1 * \Delta l_3 - 1.211 * \Delta l_1 * t_1 + 1.493 * \Delta l_1 * t_2 - 0.186 * \Delta l_1 * t_3 - 0.175 * \Delta l_1 * t_4 + 0.678 * \Delta l_1 * t_5 - 0.56 * \Delta l_1 * t_6 + 0.011 * \Delta l_2 * \Delta l_2 - 0.005 * \Delta l_2 * \Delta l_3 - 0.144 * \Delta l_2 * t_1 + 0.444 * \Delta l_2 * t_2 - 0.172 * \Delta l_2 * t_3 - 0.193 * \Delta l_2 * t_4 + 0.245 * \Delta l_2 * t_5 + 0.272 * \Delta l_2 * t_6 - 1.416 * \Delta l_3 * t_1 + 1.09 * \Delta l_3 * t_2 + 0.145 * \Delta l_3 * t_3 + 0.207 * \Delta l_3 * t_4 + 0.157 * \Delta l_3 * t_5 - 0.3 * \Delta l_3 * t_6 + 0.272 * t_1 * t_1 + 0.154 * t_1 * t_2 + 0.419 * t_1 * t_3 + 0.349 * t_1 * t_4 + 0.104 * t_1 * t_5 + 0.113 * t_1 * t_6 + 0.043 * t_2 * t_2 + 0.13 * t_2 * t_3 + 0.121 * t_2 * t_4 - 0.015 * t_2 * t_5 + 0.017 * t_2 * t_6 + 0.547 * t_3 * t_3 + 0.442 * t_3 * t_4 + 0.035 * t_3 * t_5 + 0.087 * t_3 * t_6 + 0.322 * t_4 * t_4 - 0.005 * t_4 * t_5 + 0.053 * t_4 * t_6 - 0.058 * t_5 * t_5 - 0.027 * t_5 * t_6 - 0.004 * t_6 * t_6 \quad (18)$$

$$A = 43.549 + 0.008 * \Delta l_1 + 0.012 * \Delta l_2 - 0.009 * \Delta l_3 + 0.01 * t_1 + 0.002 * t_2 + 0.001 * t_3 + 0.008 * t_4 - 0.002 * t_5 - 0.158 * \Delta l_1 * t_1 + 0.049 * \Delta l_1 * t_2 + 0.03 * \Delta l_1 * t_3 + 0.042 * \Delta l_1 * t_4 + 0.045 * \Delta l_1 * t_5 - 0.105 * \Delta l_1 * t_6 + 0.006 * \Delta l_2 * \Delta l_2 + 0.002 * \Delta l_2 * \Delta l_3 - 0.055 * \Delta l_2 * t_1 + 0.01 * \Delta l_2 * t_2 + 0.068 * \Delta l_2 * t_3 - 0.055 * \Delta l_2 * t_4 + 0.019 * \Delta l_2 * t_5 + 0.025 * \Delta l_2 * t_6 + 0.001 * \Delta l_3 * \Delta l_3 - 0.075 * \Delta l_3 * t_1 + 0.111 * \Delta l_3 * t_2 - 0.055 * \Delta l_3 * t_3 + 0.055 * \Delta l_3 * t_4 - 0.013 * \Delta l_3 * t_5 - 0.025 * \Delta l_3 * t_6 + 0.035 * t_1 * t_1 + 0.021 * t_1 * t_2 + 0.042 * t_1 * t_3 * + 0.051 * t_1 * t_4 + 0.015 * t_1 * t_5 + 0.015 * t_1 * t_6 + 0.008 * t_2 * t_2 + 0.009 * t_2 * t_3 + 0.024 * t_2 * t_4 + 0.001 * t_2 * t_5 + 0.003 * t_2 * t_6 + 0.012 * t_3 * t_3 + 0.04 * t_3 * t_4 - 0.006 * t_3 * t_5 + 0.001 * t_3 * t_6 + 0.064 * t_4 * t_4 + 0.007 * t_4 * t_5 + 0.012 * t_4 * t_6 - 0.005 * t_5 * t_5 - 0.002 * t_5 * t_6 \quad (19)$$

$$C_l = -0.0011 * \Delta l_1 + 0.0017 * \Delta l_2 - 0.0015 * \Delta l_3 - 0.0008 * \Delta \mathrm{dy} + 0.0002 * \Delta l_2 * \Delta l_2 + 0.0001 * \Delta l_3 * \Delta l_3 + 0.0002 * \Delta d_y * \Delta d_y \quad (20)$$

In summary, the dynamic relaxation factor constraint ATC method is used to build a multidisciplinary optimization design platform for the engineering problem and optimize it. The Non-dominated Sorting Genetic Algorithm II (NSGA-II) algorithm is used for the system level and the NLPQL algorithm is used for each subsystem. The specific process is shown in Figure 14.

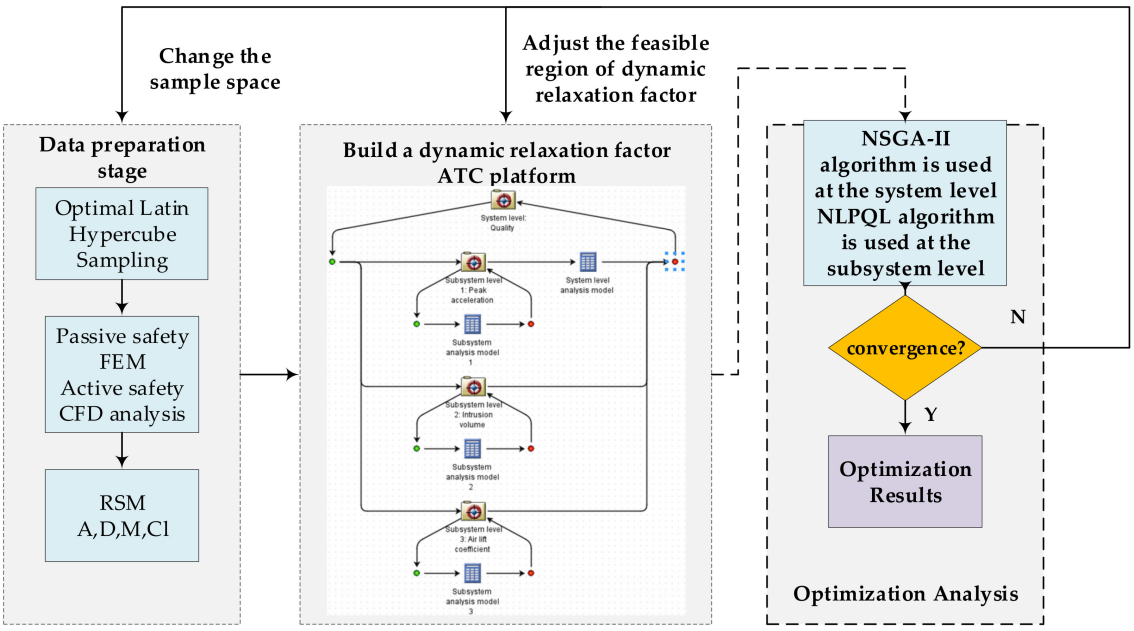

Figure 14. Construction of multidisciplinary optimization platform for engineering problems.

The optimized iterative diagram of the vehicle mass M, the intrusion D, the peak acceleration A, and the air lift coefficient C_l by numerical calculation is shown in Figure 15a–d.

After solving by MDO, compare the solved data with the initial results, as shown in Table 6. The reduction effect is represented as "-" in the table.

Table 6. Data comparison before and after optimization.

Response Value	Initial Value	Optimized Value	Improvement Effect
M/kg	46.76	43.71	−6.50%
A/g	53.42	46.96	−12.09%
D/mm	70.62	50.02	−29.18%
C_l	0.24	0.21	−12.50%

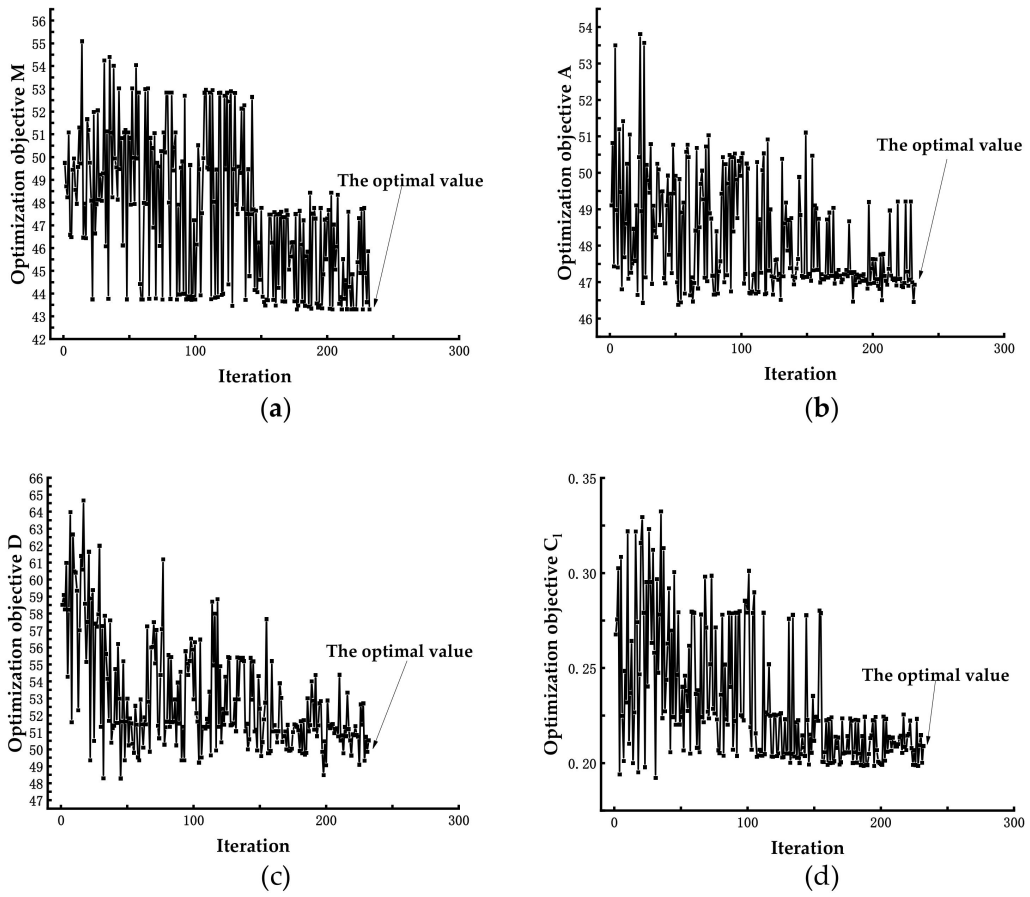

Figure 15. The optimized iterative diagram; (**a**) the vehicle mass *M*; (**b**) the peak acceleration *A*; (**c**) the intrusion *D*; (**d**) the air lift coefficient C_l.

It can be concluded from the table that before and after optimization, the body weight is reduced by 6.50%, while the peak acceleration is reduced by 12.09%, the intrusion is reduced by 29.18%, and the air lift coefficient is reduced by 12.50%. This confirms the value of the dynamic relaxation factor ATC method in practical application of engineering problems.

4. Conclusions

In this paper, the shortcomings of ATC method such as poor convergence and long iteration time are researched. The novel ATC method based on dynamic relaxation factor is proposed by adding a dynamic relaxation factor that is adjusted by the deviation of the linking variables between the levels to ensure the feasible region of the design space. The optimization framework of this method is as follows: the polynomial response surface model is used to construct the approximate model, the dynamic relaxation factor constraint is applied to the tolerance of the linking variables between levels, and the NSGA- II algorithm and the NLPQL algorithm are used for the system level and subsystem level, respectively, for the complex problems. When the dynamic relaxation factor constraint ATC method is used to solve the problem, its convergence is obviously better than that of the fixed relaxation factor constraint, which provides a method for avoiding the convergence difficulty of ATC method.

In order to ensure the application value of the ATC method in engineering practice, this paper researches the lightweight of the trussed body front impact structure based on active and passive safety. The peak acceleration and the intrusion are used as the response values to evaluate the passive safety and the air lift coefficient is used as the response value to evaluate the active safety. Compared with the traditional lightweight design that only considers passive safety, this paper reasonably associates active safety and passive

safety through the body structure. After that, the platform of dynamic relaxation factor constrained ATC method is built, each response model is fitted by RSM, the NSGA-II algorithm and the NLPQL algorithm are used for the system level and subsystem level, respectively. Compared with the initial value, the body weight is reduced by 6.50%, the peak acceleration is reduced by 12.09%, the intrusion is reduced by 29.18%, and the air lift coefficient is reduced by 12.50%. It is useful for studying the lightweight of the body structure while improving the active and passive safety. It is proved that the dynamic relaxation factor ATC method is effective in engineering practice.

However, the accuracy of the response surface approximation model method used in this paper is relatively low. Therefore, higher accuracy approximate model methods, such as reinforcement learning and deep learning, will be used in the future to improve the optimization results.

Author Contributions: Methodology, M.W.; software, M.W.; validation, T.W. and M.W.; formal analysis, X.L.; writing—original draft preparation, M.W.; writing—review and editing, T.W.; visualization, T.W.; supervision, D.Q.; project administration, T.W.; funding acquisition, T.W. All authors have read and agreed to the published version of the manuscript.

Funding: This research was funded by the National Natural Science Foundation of China—Research on the integrated design method of structure-material-performance of automobile body based on big data (51705468).

Institutional Review Board Statement: Not applicable.

Informed Consent Statement: Not applicable.

Data Availability Statement: Not applicable.

Conflicts of Interest: The authors declare no conflict of interest.

References

1. Coppola, L.; Marco, B.D.; Niola, V. Impact Attenuator Optimum Design for a FSAE Racing Car by Numerical and Experimental Crash Analysis. *Int. J. Automot. Technol.* **2020**, *21*, 1339–1348. [CrossRef]
2. Hetawal, S.; Gophane, M.; Ajay, B.K. Aerodynamic Study of Formula SAE Car. In Proceedings of the 12th Global Congress on Manufacturing and Management, Vellore, India, 8–10 December 2014.
3. Boria, S. Behaviour of an Impact Attenuator for Formula SAE Car under Dynamic Loading. *Int. J. Veh. Struct. Sys.* **2010**, *2*, 45–53. [CrossRef]
4. Xiong, F.; Wang, D.; Ma, Z. Lightweight optimization of the front end structure of an automobile body using entropy-based grey relational analysis. *Proc. Inst. Mech. Eng. D-J. Aut.* **2019**, *233*, 917–934. [CrossRef]
5. Xie, H.; Wang, P.; Wang, H. Lightweight design for an electric vehicle front cabin. *J. Plast Environ. Eng.* **2018**, *25*, 1–7.
6. Mages, M.; Seyffert, M.; Class, U. Analysis of the pre-crash benefit of reversible belt pre- pretensioning in different accident scenarios. In Proceedings of the 22nd International Technical Conference on the Enhanced Safety of Vehicles (ESV) National Highway Traffic Safety Administration, Washington, DC, USA, 20–22 April 2011.
7. Woitsch, G.; Sinz, W. Influences of pre-crash braking induced dummy—Forward displacements on dummy behaviour during EuroNCAP frontal crashtest. *Acc. Anal. Prev.* **2014**, *62*, 268–275. [CrossRef]
8. Jeongmin, C.; Kunsoo, H. Active Front Steering for Driver's Steering Comfort and Vehicle Driving Stability. *Int. J. Automot. Technol.* **2019**, *20*, 589–596.
9. Wu, W.; Zou, D.; Ou, J. Adaptive Cruise Control Strategy Design with Optimized Active Braking Control Algorithm. *Math. Probl. Eng.* **2020**, *2020*, 1–10. [CrossRef]
10. Narjes, A.; Alireza, K.; Pouria, S. Adaptive yaw stability control by coordination of active steering and braking with an optimized lower-level controller. *Int. J. Adapt. Control* **2020**, *34*, 1242–1258.
11. Sujuan, S.; Dong, J.; Chuan, B.O. Multiobjective Optimization of Nonlinear Active Suspension System with Time-Delayed Feedback. *Math. Probl. Eng.* **2020**, *2020*, 1–11.
12. Yu, Z. *The Theory of Automobile*, 5th ed.; China Machine Press: Beijing, China, 2009; pp. 138–139.
13. Roulo, D.; Ptasienski, Z.; Mccumber, B. NASCAR Truck Aerodynamic Analysis and Improvement. In Proceedings of the ASME 2017 International Mechanical Engineering Congress and Exposition, Tampa, FL, USA, 3–9 November 2017.
14. Xiang, Z.; Zhi, J.; Huang, J. A systematic approach for streamlined head form design and evaluation of Chinese high-speed train. *Int. J. Rail Transp.* **2019**, *7*, 117–139. [CrossRef]
15. Chen, Z.; Liu, T.; Jiang, Z.; Guo, Z. Comparative analysis of the effect of different nose lengths on train aerodynamic performance under crosswind. *J. Fluid Struct.* **2018**, *78*, 69–85. [CrossRef]

16. Li, R.; Xu, P.; Peng, Y. Multi-objective optimization of a high-speed train head based on the FFD method. *J. Wend Eng. Ind. Aerod.* **2016**, *152*, 41–49. [CrossRef]
17. Yu, M.; Pan, Z.; Jiang, R. Multi-objective optimization design of the head shape of high-speed train based on approximate model. *J. Mech. Eng.* **2019**, *55*, 178–186.
18. Tijssens, M.; Bosma, F.; Kietlinski, K. A Methodology and Tool Chain to Develop Integrated Safety Systems. In Proceedings of the 24th International Technical Conference on the Enhanced Safety of Vehicles (ESV), Gothenburg, Sweden, 8–11 June 2015.
19. Schoeneburg, R.; Breitling, T. Enhancement of Active and Passive Safety by Future PRE-SAFE Systems. In Proceedings of the International Technical Conference on the Enhanced Safety of Vehicles, Washington, DC, USA, 6–9 June 2015.
20. Giesing, J.P.; Barthelemy, J.M. *A Summary of Industry MDO Application and Needs*; NASA: Washington, DC, USA, 1998.
21. Dexl, F.; Hauffe, A.; Wolf, K. Multidisciplinary multi-objective design optimization of an active morphing wing section. *Struct. Multidiscipl. Optim.* **2020**, *62*, 2423–2440. [CrossRef]
22. Anselma, P.G.; Niutta, C.B.; Mainini, L. Multidisciplinary design optimization for hybrid electric vehicles: Component sizing and multi-fidelity frontal crashworthiness. *Struct. Multidiscipl. Optim.* **2020**, *62*, 2149–2166. [CrossRef]
23. Hirschler, T.; Bouclier, R.; Duval, A. Isogeometric sizing and shape optimization of thin structures with a solid-shell approach. *Struct. Multidiscipl. Optim.* **2019**, *59*, 767–785. [CrossRef]
24. Martin, I.; Hartwig, L.; Bestle, D. A multi-objective optimization framework for robust axial compressor airfoil design. *Struct. Multidiscipl. Optim.* **2019**, *59*, 1935–1947. [CrossRef]
25. Denis, V.; Chirkov, A.S.; Ankudinova, A.E. Skorospelov. Multi-objective shape optimization of a hydraulic turbine runner using efficiency, strength and weight criteria. *Struct. Multidiscipl. Optim.* **2018**, *58*, 627–640.
26. Cramer, E.J.; Dennis, J.E.; Frank, P.D. Problem formulation for multidisciplinary optimization. *SIAM J. Optim.* **1994**, *4*, 754–776. [CrossRef]
27. Haftka, R.T. Simultaneous analysis and design. *AIAA J.* **1985**, *7*, 1099–1103. [CrossRef]
28. Balling, R.J.; Sobieszczanski-Sobieski, J. Optimiza-tion of coupled systems: A critical overview of approaches. *AIAA J.* **1996**, *34*, 6–17. [CrossRef]
29. Sobieszczanski-Sobieski, J. *Optimization by Decomposition: A Step Form Hierarchic to Non-Hierarchic Systems*; NASA: Washington, DC, USA, 1989.
30. Kroo, J.; Altus, S.; Sobieszczanski-Sobieski, J. *Multidisciplinary Optimization Methods for Aircraft Prelimin-Ary Design*; NASA: Washington, DC, USA, 1994.
31. Sobieszczanski-Sobieski, J.; Agte, J.; Robert, S.R. *Bi-Level Integrated System Synthesis (Bliss)*; NASA: Washington, DC, USA, 1998.
32. Michelena, N.; Kim, H.M.; Papalambros, P.Y. A System Partitioning and Optimization Approach to Target Cascading. In Proceedings of the 12th International Conference on Engineering Design, Munich, Germany, 24–26 August 1999.
33. Yao, W.; Wu, Y.; Chen, F. A concurrent subspace collaborative optimization architecture to structural synthetical optimization design. *Struct. Multidiscipl. Optim.* **2016**, *53*, 1197–1207. [CrossRef]
34. Shin, M.K.; Park, G.J. Multidisciplinary design optimization based on independent subspaces. *Int. J. Numer. Meth. Engng.* **2005**, *64*, 599–617. [CrossRef]
35. Kim, H.M.; Rideout, D.G.; Papalambros, P.Y. Analytical target cascading in automotive vehicle design. *J. Mech. Des.* **2003**, *125*, 481–489. [CrossRef]
36. Braun, R.; Gage, P.; Kroo, I. *Implementation and Performance Issues in Collaborative Optimization*; American Institute of Aeronautics and Astronautics: Reston, VA, USA, 1996.
37. Li, X.; Li, W.; Liu, C. Geometric analysis of collaborative optimization. *Struct. Multidiscipl. Optim.* **2008**, *35*, 301–313. [CrossRef]
38. Precup, R.; David, R.; Roman, R. Slime Mould Algorithm-Based Tuning of Cost-Effective Fuzzy Controllers for Servo Systems. *Int. J. Comput. Int. Syst.* **2021**, *14*, 1042–1052. [CrossRef]
39. Zapata, H.; Perozo, N.; Angulo, W. A Hybrid Swarm Algorithm for Collective Construction of 3D Structures. *Int. J. Artif. Intell.* **2020**, *18*, 1–18.
40. Roman, R.; Precup, R.; Bojan-Dragos, C. Combined Model-Free Adaptive Control with Fuzzy Component by Virtual Reference. Feedback Tuning for Tower Crane Systems. *Procedia Comput. Sci.* **2019**, *162*, 267–274. [CrossRef]
41. Fatma, G.; Islem, L.; Chiraz, H. Optimization of boron removal from water by electrodialysis using response surface methodology. *Water Sci. Technol.* **2020**, *81*, 293–300.
42. Srinivas, G.R.; Deb, A.; Sanketh, R. An Enhanced Methodology for Lightweighting a Vehicle Design Considering Front Crashworthiness and Pedestrian Impact Safety Requirements. *Adv. Mat. Res.* **2017**, *173*, 623–630. [CrossRef]
43. Xiong, J.; Li, T.; Zhang, J. Shape optimization of high-speed trains under multi running conditions. *Sci. China Technol. Sci.* **2016**, *46*, 313–322.
44. Muñoz-Paniagua, J.; García, J.; Crespo, A. Genetically aerodynamic optimization of the nose shape of a high-speed train entering a tunnel. *J. Wind Eng. Ind. Aerod.* **2014**, *130*, 48–61. [CrossRef]